FUKUSHIMA DAIICHI UNIT 1 EX-VESSEL PREDICTION: CORE MELT SPREADING

M. T. Farmer
Argonne National Laboratory
9700 S. Cass Avenue, Argonne, IL 60439, USA
farmer@anl.gov

K. R. Robb and M. W. Francis
Oak Ridge National Laboratory
P.O. Box 2008, Oak Ridge, TN 37830, USA
robbkr@ornl.gov, francismw@ornl.gov

ABSTRACT

Lower head failure and corium-concrete interaction were predicted to occur at Fukushima Daiichi Unit 1 (1F1) by several different system-level code analyses, including MELCOR v2.1 and MAAP5. Although these codes capture a wide range of accident phenomena, they do not contain detailed models for ex-vessel core melt behavior. However, specialized codes exist for analysis of ex-vessel melt spreading (e.g., MELTSPREAD) and long-term debris coolability (e.g., CORQUENCH). On this basis, an analysis has been carried out to further evaluate ex-vessel behavior for 1F1 using MELTSPREAD and CORQUENCH. Best-estimate melt pour conditions predicted by MELCOR v2.1 and MAAP5 were used as input. MELTSPREAD was then used to predict the spatially-dependent melt conditions and extent of spreading during relocation from the vessel. This information was then used as input for the long-term debris coolability analysis with CORQUENCH that is reported in a companion paper.

KEYWORDS
Fukushima, severe accident, ex-vessel, spreading

1. INTRODUCTION

MELCOR simulations for Fukushima Daiichi Unit 1 (1F1), carried out as a part of a joint effort between the Department of Energy (DOE-NE) and the Nuclear Regulatory Commission (NRC) Fukushima Daiichi Accident Study [1], predict major core melting, bottom head failure, and corium-concrete interaction. These predictions are in agreement with simulations performed by the Electric Power Research Institute (EPRI) using the MAAP code [2], as well as the former Japanese Nuclear Energy Safety Organization (JNES) using MELCOR [3] and the Tokyo Electric Power Company (TEPCO) using MAAP [3,4]. Vessel failure has also been predicted through simulations with the European severe accident code ASTEC V2.0 [5]. Additionally, containment atmospheric monitoring system (CAMS) and reactor pressure vessel (RPV) temperature data as well as energy balance analysis suggest that melt has exited the RPV [6-8]. Both MELCOR and MAAP are capable systems-level modeling tools that capture a wide spectrum of accident phenomena in a tractable manner. However, for ex-vessel sequences, specialized codes containing more detailed modeling are available for the analysis of melt spreading (e.g., MELTSPREAD [9,10]), as well as debris coolability during molten corium-concrete interaction (e.g., CORQUENCH [11,12]). This paper summarizes the results of MELTSPREAD analyses of ex-vessel core debris relocation behavior in 1F1 [13]. Information from this study provides the initial and boundary

conditions for analyzing long-term core debris cooling behavior with CORQUENCH, the results of which are documented in a companion paper [13,14].

With this background, the overall objective of this work is to utilize MELTSPREAD to provide more rigorous, best-estimate predictions and analysis of ex-vessel core melt accident relocation following postulated vessel failure at 1F1 based on best-estimate melt pour conditions from MELCOR [1] and MAAP [2] simulations. Other general goals of the study are to: i) provide results for comparison against MELCOR and/or MAAP results, ii) scope out the range of possible final debris locations in containment, and iii) identify uncertainties in the predictions.

In terms of approach, melt pour conditions following RPV failure obtained from the MELCOR [1] and MAAP [2] analyses were used as input to MELTSPREAD to generate predictions of melt spreading, basemat attack, cladding oxidation (viz. H_2/CO production), debris cooling, and drywell liner attack during the transient spreading phase. One of the principal outcomes of this analysis was the extent of floor coverage during spreading, which is important since the depth of debris to be cooled in the long term is inversely proportional to the floor area covered by melt. Since cavity conditions during the accident are uncertain, a sensitivity study was performed to evaluate the effect of the presence/absence of water on the cavity floor, melt pour rate and temperature, and sump cover plate failure on the global spreading behavior. MELTSPREAD and CORQUENCH are two separate and distinct computer codes. Thus, MELTSPREAD was used to define tabular input for CORQUENCH, which in turn evaluated the long-term debris cooling behavior [13,14].

An outline for the balance of this work is as follows. A brief summary of MELTSPREAD modeling capabilities, improvements, and validation status is provided first, followed by a description of the case scenarios and modeling assumptions used in the 1F1 analysis. The main results are then presented, followed by a summary of key findings from this study.

2. MELTSPREAD DESCRIPTION

MELTSPREAD was originally developed to support resolution of the Mark I shell vulnerability issue [15]. Given the melt pour conditions (i.e., temperature, composition, and flow rate), the code solves the 1-D momentum equation to evaluate melt spreading depth and velocity while accounting for local core debris cool down and solidification, concrete heat-up and decomposition, metals oxidation from concrete decomposition gases, and heat transfer to overlying atmosphere under both wet and dry cavity conditions. The code treats melt compositions ranging from fully metallic to fully oxidic. In addition, the code can calculate heat-up of structure adjacent to (or in the pathway of) flowing core debris. This model was specifically developed to examine heat-up of the Mark I shell under conditions in which the core debris was calculated to contact that structure.

MELTSPREAD was extensively updated and validated for application to spreading in the European Pressurized Reactor core catcher design [16]. Property routines in the original code were only capable of treating mixtures of core and cladding metals and their corresponding oxides, and only substrates composed of concrete and/or steel. Thus, one of the first improvements was to provide the ability to input simulant melt and/or substrate material properties. This allowed all simulant material spreading tests reported in the literature to be calculated, as well as tests with ceramic substrate.

Another key improvement in the area of material properties was to incorporate the ability to input a tabular function for the oxide-phase solid fraction variation between the liquidus and solidus temperatures. Originally the oxide-phase solid fraction was treated as varying linearly in this range, but subsequent research has shown that the solid fraction is highly nonlinear for multi-component oxide melts

[17]. Since solid fraction has a key effect on viscosity which, in turn, strongly affects spreading behavior, this was one of the most important improvements to the code in the area of material properties evaluation.

The capability to carry out inviscid and/or adiabatic spreading analysis was also added, so that analytical solutions as well as isothermal spreading tests could be calculated by appropriate selection of input data. The ability to model interfacial heat transfer resistance at the melt-substrate interface was also added; this is important in terms of calculating spreading and solidification of metallic melts for which shrinkage at the melt–substrate interface can have a marked effect on the local heat transfer rate [16]. Finally, the code was updated to include a new correlation for melt viscosity that was found to better reproduce spreading behavior over a wide range of conditions (see Ramacciotti et al. [18]).

A key element of the validation process was to assemble a set of test cases against which the code could be compared to check the accuracy of the numerical algorithms and to determine the extent to which the model can reproduce actual spreading behavior [16]. A total of 35 different cases were calculated as part of the code validation exercise, including: i) the analytical solution to dam break problem (one case), ii) isothermal tests (six cases), and finally iii) flow and freezing tests (28 cases); that is, core oxides (seven tests), core oxide–steel mixtures (four tests), simulant oxides (12 tests), and steel alone (five tests). Details are provided in [16].

3. SUMMARY OF CASE SCENARIOS AND MODELING ASSUMPTIONS

As noted, MELCOR v2.1 [1] and MAAP5 [2] were independently exercised as part of US efforts to evaluate the 1F1 plant response during the accidents initiated on 11 March 2011. These analyses were carried out up through the point of reactor vessel failure and discharge of the core melt into the reactor containment. Key input relevant to the current study deduced from MELCOR and MAAP5 output are summarized in Table I.

The MELCOR scenario [1] is a low-pressure sequence in which the vessel is predicted to fail at 14.27 hours, leading to the gradual discharge of ~ 141 MT of core debris into the drywell over the course of 67 minutes. MELCOR predicts the water depth in the drywell to be ~55 cm at RPV failure. The debris pour rate is highest right after the vessel fails, averaging 205 kg/sec over the first seven minutes of the transient. The balance of the material (53 MT) relocates over the following hour at varying rates, all of which are less than the initial rate. (The time-dependent flow rate was mocked up as part of the MELTSPREAD input). The debris temperature distribution in the lower head just before the vessel fails ranges from 1850 to 2100 K. For this study an average temperature of 1975 K was assumed. The melt composition consists primarily of core oxide (UO_2-ZrO_2) with ~ 43% of the cladding oxidized. The debris contains ~ 20 wt% structural steel. Given this debris temperature range, the metal phase is predicted to be fully liquid, while the oxide is predicted to be fully solid. The resultant solids content in the core mixture at vessel failure is thus estimated as ~ 56 vol% (see Table I). The melt is expected to be quite viscous with this level of solids. The decay heat in the debris at vessel failure is equivalent to 86 W/kg fuel.

The MAAP analyses [2] considered both low-pressure (MAAP-LP) and high-pressure (MAAP-HP) scenarios (Table I). For the low-pressure case, the vessel fails at 10.11 hours, leading to rapid discharge of ~140 MT of core debris into the pedestal within ~ 18 seconds. The water depth in the drywell for this sequence is ~ 20 cm at vessel failure. The average pour rate over the relocation transient is ~ 8 MT/sec, which is ~40 times larger than the flow rate predicted by MELCOR. The debris temperature at vessel failure is 2751 K; thus, the melt is superheated by ~160 K relative to the oxide phase liquidus. As for the MELCOR case, the melt composition is primarily of core oxide, but with slightly less cladding oxidation (i.e., 39 % vs. 43 % for MELCOR). The debris also contains ~ 20 wt% structural steel, but MAAP predicts much higher structural steel oxidation leading to the presence of ~11 MT of iron oxide (FeO) in the melt. As noted earlier, the melt is superheated with respect to both the oxide and liquid phase; thus,

the core debris is completely fluid during relocation. This case contrasts with the predicted MELCOR pour stream that contains a high solid content (56 vol%). Based on the MAAP analysis, decay heat in the debris at vessel failure at 10.11 hours is ~ 96 W/kg fuel.

Table I. Melt spreading input data from MELCOR [1] and MAAP [2] accident analyses

Case Designator	MELCOR	MAAP-LP	MAAP-HP
Sequence description	LP vessel failure	LP vessel failure	HP vessel failure
Onset of pour (hours)	14.27	10.11	8.14
Pour duration (sec)	4030	17.5	5.3
Containment pressure (MPa)[b]	0.75	0.75	0.75
Water level on drywell floor (cm)	55	20	0
Melt pour temperature (K)	Range: 1850-2100 Average: 1975	2751	2797
Oxide phase solidus-liquidus (K)[a]	2215-2467	1934-2588	1925-2587
Metal phase solidus-liquidus (K)[a]	1705-1735	1802-1812	1803-1813
Melt solid fraction (-)[a]	0.56	0.0	0.0
Decay heat (W/kg fuel)	86	96	105
Pour mass of constituent (kg)			
UO_2	69400	76153.2	76153.4
Zr	25800	16594.1	16616.0
ZrO_2	16600	14141.5	14112.7
Cr	5900	1135.9	1099.4
Cr_2O_3	30	2732.0	2765.5
Fe	20430	16095.1	15928.4
FeO	230	11210.5	11369.5
Ni	2530	555.7	534.8
NiO	30	1208.2	1229.1
B_4C	0	502.0	502.0
Total	140950	140328.3	140310.8

[a]Calculated with CORQUENCH subroutines given composition and melt pour temperature
[b]Approximate; based on plant data [13].

For the MAAP-HP scenario, the vessel fails earlier (i.e. at 8.14 hours). Pour mass and composition are similar to the LP scenario, with the exception that the melt is more superheated (i.e. 210 K vs. 160 K). The pour rate is large, ~26.5 MT/sec, which is roughly three times higher than the low-pressure sequence. There is one additional difference between the LP and HP cases; i.e., the cavity is dry during relocation for the HP case. Decay heat is also slightly higher (viz. 105 W/kg fuel) due to the earlier melt release.

As is evident from Table I (and alluded to above), there are significant differences between the predicted melt pour conditions between MAAP and MELCOR. A recent study [19] indicated that there are gaps in the existing data base for modeling BWR late-phase in-core fuel and structure degradation and relocation, especially with respect to phenomena that affect multiple assemblies. These gaps have led to differences in modeling approaches adopted by MAAP and MELCOR that strongly impact the predicted behavior. A recent code comparison activity [20] indicated that the principal phenomenological uncertainty regarding in-core behavior is the extent that core debris is permeable to gas flow during degradation. Namely, impermeable debris (assumed in MAAP) leads to gradual accumulation of a large high temperature in-core melt accumulation akin to that formed during TMI-2, while permeable debris (assumed in MELCOR) steadily relocates to the lower head where the material collects as a debris bed.

In terms of the cavity characteristics, the 1F1 containment is a Mark I design. Internal to the pedestal, there are two rectilinear drywell sumps, each 1.45 m by 1.45 m in cross-section and 1.2 m deep. The sumps are normally covered with 6.35 mm thick steel decking plates. The centerline of each sump is

offset by 1.47 m from the pedestal axial centerline. The internal radius of the pedestal wall is 2.5 m, and the wall thickness is 1.2 m. There is a doorway from the pedestal to the drywell annulus that is 1.0 m wide. The radius of the drywell shell is 6.55 m where the shell contacts the drywell floor. Due to the 1-D modeling limitations of the code, the two drywell sumps are combined into a single geometric entity that consists of cylinder located at the pedestal centerline that is 2.23 m in diameter and 1.2 m deep (see Figure 1). Thus the sump volume, cross-sectional areas, and depth are conserved as part of the nodalization. (Whether or not the sump plates fail during relocation is treated parametrically). The balance of the drywell floor from the sump edge to the pedestal inner wall is discretized into 13 cylindrical mesh cells with a uniform radial incremental of ~ 10 cm. Flow through the pedestal doorway is assumed to occur in a one-dimensional channel (the 1.2 m flow distance discretized into 12 nodes of equal size). Outside the pedestal doorway, the core melt is assumed to spread in a 90º sector to the shell; the total distance of 2.85 m from the pedestal outer wall to the shell is discretized into 28 nodes of equal size (10 cm). After the melt contacts the liner, the flow is assumed to be diverted *symmetrically* into the two sides of the drywell annulus. A courser discretization was used in this region; i.e. 28 nodes were employed resulting in a uniform cell size of 47 cm long (in a 1-D channel approximation). Regarding the potential for shell heatup by impinging melt, the options for calculating this behavior were invoked for this study. Details regarding the shell nodalization scheme and heat transfer modeling assumptions are provided in [13].

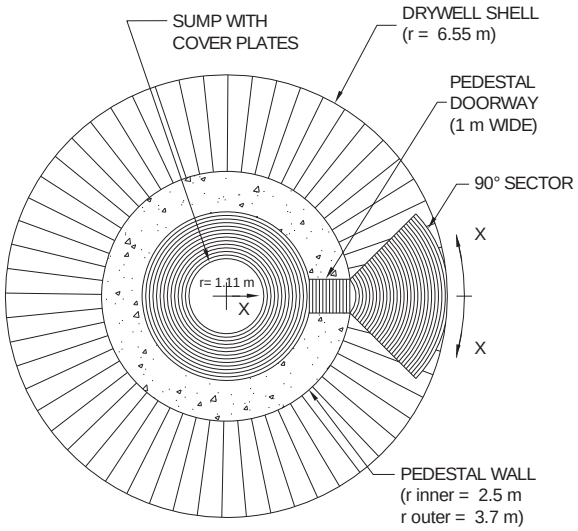

Figure 1. Containment Nodalization Scheme.

Below-vessel structure is extensive in BWRs, primarily consisting of control rod drives and instrument tube penetrations, as well as a catwalk for personnel access to this equipment. These structures may impact the melt relocation behavior, causing flow diversion and possibly creating a rain-drop effect that can reduce impingement heat transfer. Analysis of this type of behavior is beyond the current scope of work. A previous study [21] indicated that lower structures do not have a dominating effect on melt relocation. As such, the melt is assumed to relocate directly into the drywell sump (modeled as a single discrete mesh cell), and spread from there. Regarding other modeling limitations, water on the floor as an initial condition can affect spreading by causing melt jet fragmentation and cooling prior to impact with the floor. This effect is currently not modeled in MELSTPREAD; thus, the spreading areas reported herein for wet cavity cases are most likely over-estimated. In addition, the code does not treat water heat-up and boil-off, and so for situations in which limited water is present, the code will over-predict the cooling behavior compared to situations in which the inventory can boil off and uncover previously cooled debris. Both wet and dry scenarios are presented that should bound water-starved cases.

Although the concrete used in the construction of the Fukushima Daiichi plants is of the siliceous type, the exact composition was not known when this study was conducted. For consistency with the MELCOR study [1], the composition was set equal to the default Basalt concrete composition in MELCOR, a concrete type that is similar to siliceous.

Aside from the above described geometry modeling assumptions, MELTSPREAD input allows other options regarding heat transfer and material property modeling assumptions. As part of the code validation efforts [16], a set of best-estimate modeling assumptions were developed that minimized

differences in predicted spreading area over a wide range of tests and test conditions. These best estimate input modeling assumptions were used for all cases considered in this study; see [13].

Several cases were evaluated for each sequence in order to examine the sensitivity of the spreading behavior on several factors. The six cases that were calculated for the MELCOR sequence are summarized in Table II, while the four cases that were calculated for both the MAAP low- and high-pressure sequences are summarized in Tables III and IV, respectively. A common case scenario was established early in the process in order to provide a technical basis for systematically examining parametric effects. The common scenario assumes that water is initially present on the drywell floor, and that the depth is limited by the vent line height that is assumed to be 60 cm. Thus, for situations in which local debris depth is larger than 60 cm, the debris cools by radiation to overlying structure. However, if the melt depth is below the vent line height, the material is assumed to be cooled by heat transfer to overlying water. The sump cover plates are thin (6.4 mm) and even if they do not fail by impingement heat transfer, the ability of these plates to withstand the mechanical load of the core debris is questionable. Thus, the base case assumes that the plates fail upon contact with the core debris. Thereafter, melt accumulates in the sumps until the height exceeds the sump depth (1.2 m); thereafter the debris will start to spread on the pedestal floor.

Table II. MELCOR scenario with RPV failure at 14.27 hours

Case No.	Description/Rationale	Parameter Investigated
MELCOR-1	***Base case***: Table I melt pour conditions with 60 cm water level (limited by vent line height). Sump plates fail at t=0	-
MELCOR-2	Case 1, but sump plates initially intact (MELTSPREAD predicts insufficient thermal loading to fail the plates over the pour duration, but the code does not perform a mechanical load limit analysis).	Melt retention in sump
MELCOR-3	Case 1, but the cavity is dry. It is not clear that there was coolant leakage into containment before RPV failure (aside from steam venting into torus through the SRVs).	Dry cavity
MELCOR-4	Case 1, but cavity water level is limited to ½ the vent line height (30 cm).	Water depth
MELCOR-5	Case 1, but melt assumed to accumulate in lower head and relocate in 10 seconds. Melt release rate from the vessel is a modeling uncertainty.	Melt pour rate
MELCOR-6	Case 3, but melt assumed to accumulate in lower head and relocate in 10 seconds.	Dry cavity & pour rate

Table III. MAAP-LP scenario with vessel failure at 10.11 hours

Case No.	Description/Rationale	Parameter Investigated
MAAP-LP-1	Case 4, but cavity water level limited to the vent line height (60 cm)	Water depth
MAAP-LP-2	Case 4, but the sump plates are initially intact (rapid plate ablation and failure is predicted by 4.37 seconds for this scenario).	Melt retention in sump
MAAP-LP-3	Case 4, but the cavity is dry. It is not clear that there was coolant leakage into containment before RPV failure (aside from steam venting into torus through the SRVs).	Dry cavity
MAAP-LP-4	***Base case***: Table I melt pour conditions with 30 cm water level (½ the vent line height). Sump plates fail at t=0.	-

Table IV. MAAP HP scenario with vessel failure at 8.14 hours

Case No.	Description/Rationale	Parameter Investigated
MAAP-HP-1	Case 3, but cavity water level is limited to the vent line height (60 cm).	Water depth
MAAP-HP-2	Case 3, but the sump plates are initially intact (rapid plate ablation and failure is predicted by 3.58 seconds for this scenario) and the water level is limited to the vent line height (60 cm).	Melt retention in sump
MAAP-HP-3	***Base case***: Table I melt pour conditions; sump plates fail at t=0; cavity is dry.	-
MAAP-HP-4	Case 3, but cavity water level limited to ½ the vent line height (i.e. 30 cm).	Water depth

MELTSPEAD has the ability to analyze heat up and ablation of the sump cover plates as a modeling option. The structural support system for these thin plates is not known, and so early mechanical failure cannot be assumed for all situations. Thus, case two for all three scenarios utilizes the sump cover heat up and ablation model to determine if the plates are predicted to fail by impingement heat transfer and, if not, what the effect of debris relocation is over these plates on the spreading behavior. The third case is equivalent to the first case, but the cavity is assumed to be dry during relocation. Thus, this case examines the effect of a wet vs. dry cavity floor on the spreading behavior. The fourth case is equivalent to the first case, but the water depth is reduced to ½ the vent line height (i.e. 30 cm). Thus, cases 1, 3 and 4 together parameterize on the water depth during the spreading transient, ranging from initially dry to the situation in which the depth is limited by the vent line height.

As described earlier, differences in the MELCOR and MAAP pour conditions are considerable. The conditions range from a slow, gradual pour of a viscous low-temperature melt (MELCOR scenario) to the rapid pour of a superheated core material (MAAP scenarios). Thus, two additional cases were calculated for the MELCOR sequence in which a very rapid pour of a low temperature melt occurs over a compressed time scale of 10 seconds. This type of situation would be indicative of a global lower head creep rupture scenario where the head weakens and eventually fails catastrophically, leading to rapid discharge of the core debris into the containment. Case 5 is the same as the base case, but with the pour duration shortened to 10 seconds. Case 6 is the same as case 5, but the sump cover plates are assumed to remain intact during relocation. Thus, case 6 is considered to be a worst case scenario for liner attack based on the MELCOR results.

4. RESULTS

4.1 MELCOR Pour Scenario

According to the MELTSPREAD property routines, the viscosity of the core debris at the stated pour conditions (Table I) is ~77 Pa·sec at the vessel exit temperature of 1975 K, which is the same order-of-magnitude as chocolate syrup or ketchup.[1] Under these conditions the flow is expected to be dominated by viscous effects. MELCOR predicts that the water depth on the pedestal floor at vessel failure is ~ 55 cm (Table I). Thus, the best estimate calculation is selected to be the MELCOR-1 case in which the sump plates fail at contact with core debris, and the material spreads under water at a depth limited by the vent line height of ~ 60 cm. Plots showing the melt height and temperature distributions at various times following vessel failure for this case are provided in Figure 2 (see Figure 1 for the coordinate system used in this and other figures). In addition, melt leading edge location, depth adjacent to the drywell shell[2], and peak shell temperature for all six MELCOR cases (see Table II) are shown collectively in Figure 3.

In the base case, the melt gradually fills the sump volume and then begins to spread first in the pedestal region and then out the pedestal doorway, making contact with the shell at ~182 seconds. After contacting the shell the flow is diverted (symmetrically by assumption) into the annulus where the debris travels a small distance (~50 cm) before relocation is halted by freezing at the leading edge. This corresponds to the end of the spreading transient after the initial 7 minute pour phase; see Figure 3 and depth/temperature plot at 700 seconds in Figure 2. The debris profile at this point consists of a fairly uniform layer of core debris in the 20-30 cm depth range (some molten, some frozen); the material in the sump is ~ 150 cm deep due to the elevation difference.[3] Due to the high viscosity and low spreading velocity of the material, convective heat transfer to underlying concrete is small. As a result, the code

[1] See e.g. http://en.wikipedia.org/wiki/Viscosity

[2] The shell is inclined at ~ 45º; thus, shell distance covered by melt is equal to the square root of two times the local melt depth.

[3] When debris locally solidifies, it is incorporated into the basemat and the volume reduction upon solidification is calculated (~ 20%); this is reflected in the height reductions in Figures 2-3 between 500 and 700 seconds. The instantaneous reductions in debris depth adjacent to the shell in Figure 3 are due to the same affect.

predicts essentially no concrete ablation during spreading (although there is concrete degasing due to local heat up in the thermal boundary layer).

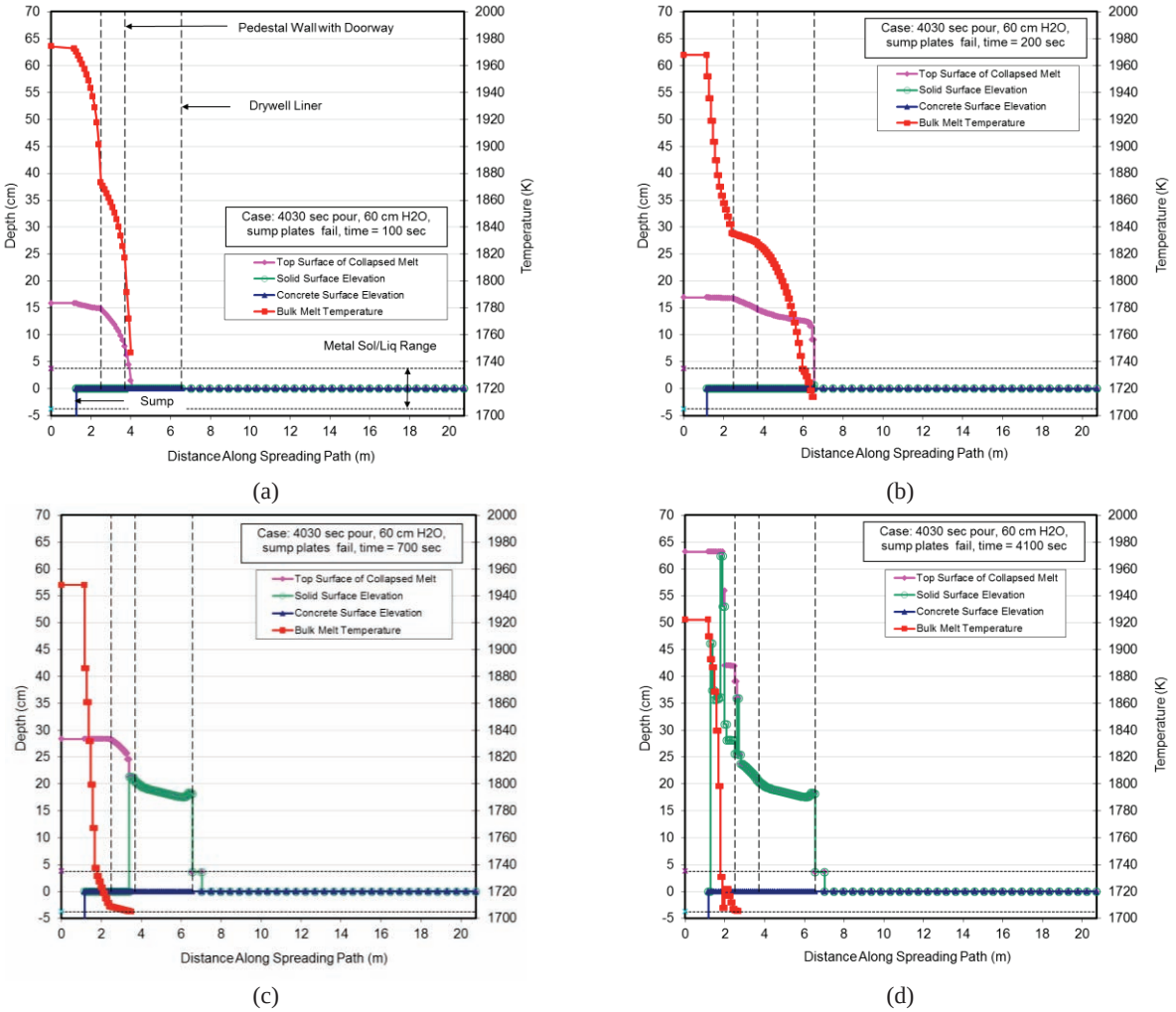

Figure 2. (a-d) Temperature-Depth Profiles at 100, 200, 700, and 4100 sec for MELCOR-1 Case.

Over the next 50 minutes, core debris gradually drains from the pressure vessel, and some of this material spreads out the pedestal doorway where it freezes over the previously frozen debris. However, the vast majority of this new material is retained as a molten pool inside the pedestal region. The final significant debris relocation transient of ~ 28 MT from 3500 to 4030 seconds leads to the accumulation of a mound of material in the pedestal that slightly exceeds the water height of 60 cm assumed for this scenario. The final debris configuration for the best-estimate MELCOR case is thus predicted to be a mound of material ~ 63 cm deep inside the pedestal, with a lesser amount of debris outside the pedestal doorway and in contact with the shell. The final floor area coverage is ~ 33 m^2, which includes the sump.

Due to the low spreading velocity, the melt depth gradually increases adjacent to the shell (Figure 3). The shell surface temperature shows an early peak that is indicative of initial melt contact and crust growth to the quasi-steady equilibrium depth. Thereafter, the shell surface temporarily cools as heat is dissipated into the bulk of the steel. However, this heat sink is soon exhausted and the surface begins to heat up until a quasi-steady condition is reached in which heat transfer from the melt is dissipated by conduction along the shell to overlying water. The inflection point in shell surface temperature at ~350 seconds for the best estimate case (as well as the inflection points for the other cases) corresponds to the time of bulk

solidification of debris next to the shell. At this point, the heat transfer switches from convection to conduction-limited heat transfer, and so the shell surface temperature ramp is temporarily interrupted before reheating to a peak of ~1400 K at ~ 900 seconds. Thereafter, the temperature steadily declines over the balance of the calculation. Thus, the shell is predicted to remain intact for this scenario by virtue of the fact that the melting point is not reached. However, this study does not consider other potential failure modes such as creep rupture.[4]

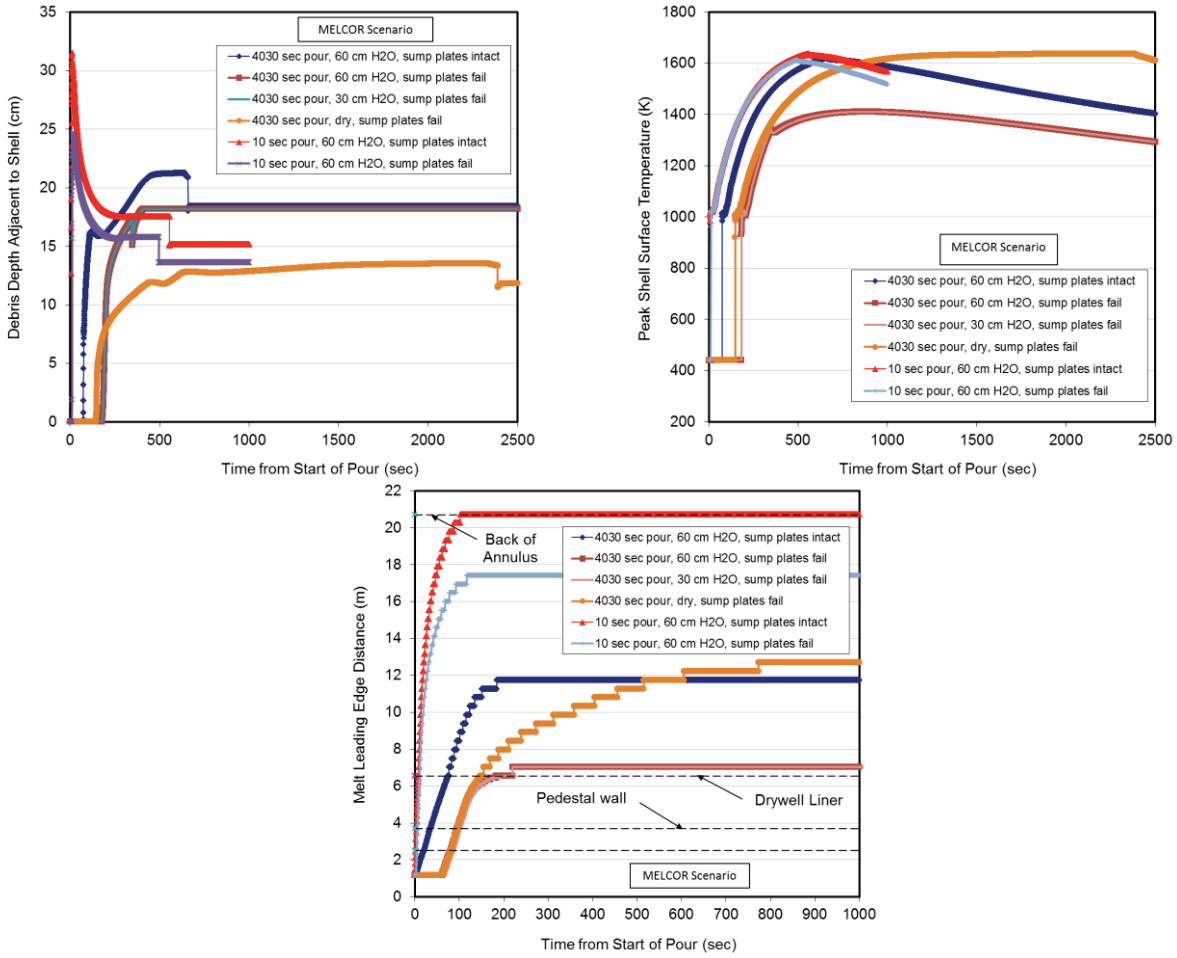

Figure 3. Clockwise from Upper Left: Melt Depth Adjacent to Shell, Peak Shell Temperature, and Melt Leading Edge Location for the Six MELCOR Cases.

Examination of Figure 3 for the other three extended pour MELCOR cases indicates that the overall spreading behavior is affected by the presence/absence of water on the drywell floor. For the dry cavity case, the final spreading area nearly doubles to 65.5 m^2 compared to the reference case. However, the depth of water in the range investigated (i.e. 30 cm vs. 60 cm) does not have a significant effect on the overall extent of spreading, although the depth of the debris retained in the pedestal was found to be reduced to ~ 50 cm for the MELCOR-4 (30 cm water depth) case. Somewhat surprisingly, the shell is predicted to remain intact for the dry case, reaching a peak temperature of 1570 K at 2400 seconds. This is due to the fact that the debris depth adjacent to the shell is reduced to ~ 13 cm for this case by virtue of the increased spreading area. For the case in which the sump plates remain intact (MELCOR-2), the melt

[4] Liner creep rupture was investigated for a single accident scenario during the Mark-I liner attack study [15]. In that work, creep rupture occurred at a failure temperature of 1511 to 1583 K (95 percent confidence bounds), but the work was carried out for a single accident scenario. Creep is a function of time, temperature, and variations in heating rate, peak temperature, and extent of liner contact with core debris, which could affect the prediction of the liner failure temperature.

makes earlier contact with the shell, but the depth of the material adjacent to the shell as well as the peak shell temperature are quite close to the best estimate case. This is due to the fact that the spreading area is nearly doubled to 60.2 m^2 in this calculation, which apparently compensates for the lack of material retention in the sump.

The results of the two cases performed to examine the effect of increased pour rate on spreading of low temperature debris (cases MELCOR-5 and -6) indicate that spreading area increases substantially relative to that seen for the low pour rate cases. Inertial effects become more important for these high flow rate cases, causing the melt to splash up on the shell outside the pedestal doorway (Figure 3). This causes earlier peaks in the shell surface temperature, but the shell is predicted to remain below the melting point. The high pour rate case without sump plate failure is the only MELCOR scenario in which the melt is predicted to fully cover the pedestal and drywell annulus floor areas.

4.2 MAAP Low Pressure Scenario

In this case, the pour stream is superheated (see Table I). According to the MELTSPREAD property routines, the melt viscosity at vessel failure is ~2 mPa·sec; this is the same order-of-magnitude as water. Due to the high flow rate and low viscosity, spreading will be dominated by inertial effects. The MAAP analysis [2] predicts a water depth on the drywell floor at vessel failure of ~ 20 cm. Thus, the best estimate calculation is selected to be the MAAP-LP-4 case (Table III) in which the sump plates fail at initial melt contact, and the material spreads under water at a depth of ~ ½ the vent line height. Plots showing the melt height and temperature distributions at various times following vessel failure are provided in Figure 4, while melt leading edge location, depth adjacent to the drywell shell, and peak shell temperature for all four MAAP-LP cases are shown collectively in Figure 5.

Due to the high pour rate and low viscosity, the melt rapidly fills the sump volume and then begins to spread out the pedestal doorway, making contact with the shell at ~12 seconds. The core melt then begins spreading throughout the annulus, eventually covering the entire floor area in ~ 30 seconds. By two minutes, sloshing has effectively ceased and the debris equilibrates at a uniform level in the pedestal/drywell at ~13 cm. The corresponding melt depth in the sump at the end of the spreading transient reaches ~ 133 cm. As is evident from Figure 4, a concrete erosion pocket forms inside the pedestal doorway and just outside this opening; the peak erosion depth reaches ~ 20 cm over two minutes. This localized ablation is due to relatively high spreading velocities achieved (approaching 3 m/sec) as the material relocates through this narrow opening into the annulus. The high velocities, in conjunction with the shallow melt depth and low viscosity, result in large convective heat transfer in this region. Cumulative concrete attack during spreading was significant for this case with ~ 2 m^3 in the first 2 minutes.

Due to the high flow rate and low viscosity, the code predicts that the melt initially washes up on the shell (Figures 4 and 5), leaving a residual crust higher up on the shell early in the transient. The shell surface temperature shows an early peak that is indicative of initial melt contact and crust growth to the quasi-steady equilibrium depth. Thereafter, the shell surface cools as heat is dissipated into the bulk of the steel. The shell reheats until a quasi-steady condition is reached where heat transferred from the melt is conducted up along the shell where it is dumped to the overlying water through boiling. The inflection point in the surface temperature response at 540 seconds corresponds to bulk solidification of material next to the shell. At this point, the heat transfer to the shell switches from convection to conduction-limited, and so the shell begins to cool slightly after reaching a peak temperature of ~1560 K, which is below the steel melting point of ~1810 K. Thus, the shell is predicted to remain intact for this scenario since the melting point is not reached. However, as noted earlier[4], this analysis does not consider other potential failure modes such as creep rupture.

Examination of Figure 4 for the other three MAAP-LP cases indicates that the overall spreading behavior is not sensitive to the presence or absence of water. This is due to the fact that the energy transport from the vessel during relocation for this high-pour rate, high temperature case overshadows achievable (i.e. CHF-limited) heat removal rates to overlying water, and so the melt is readily able to spread to a uniform melt depth. For the case in which the sump cover plates are assumed to be initially intact, the debris is able to propagate earlier into the drywell and annulus, but the plates are ablated through by 4.37 seconds. After this time, a thin melt layer continues to spread outside the pedestal doorway, while material inside the pedestal on the floor begins to flow back into the sump as the sump fills with corium draining from the vessel. The residual material in the annulus cools and seems to impede the spreading behavior later in the transient after the sump fills and material again spills out the doorway. The overall effect is found to be a slight reduction in peak shell temperature relative to that in which the sumps fail at initial melt contact.

Aside from spreading behavior, the lack of water in the drywell is found to have an effect on shell heat up. For the dry case, the peak shell temperature had reached 1650 K at the end of the computed time interval (750 seconds), and is still rising. Thus, the current analysis predicts that shell failure would be likely for a dry low-pressure MAAP pour scenario.

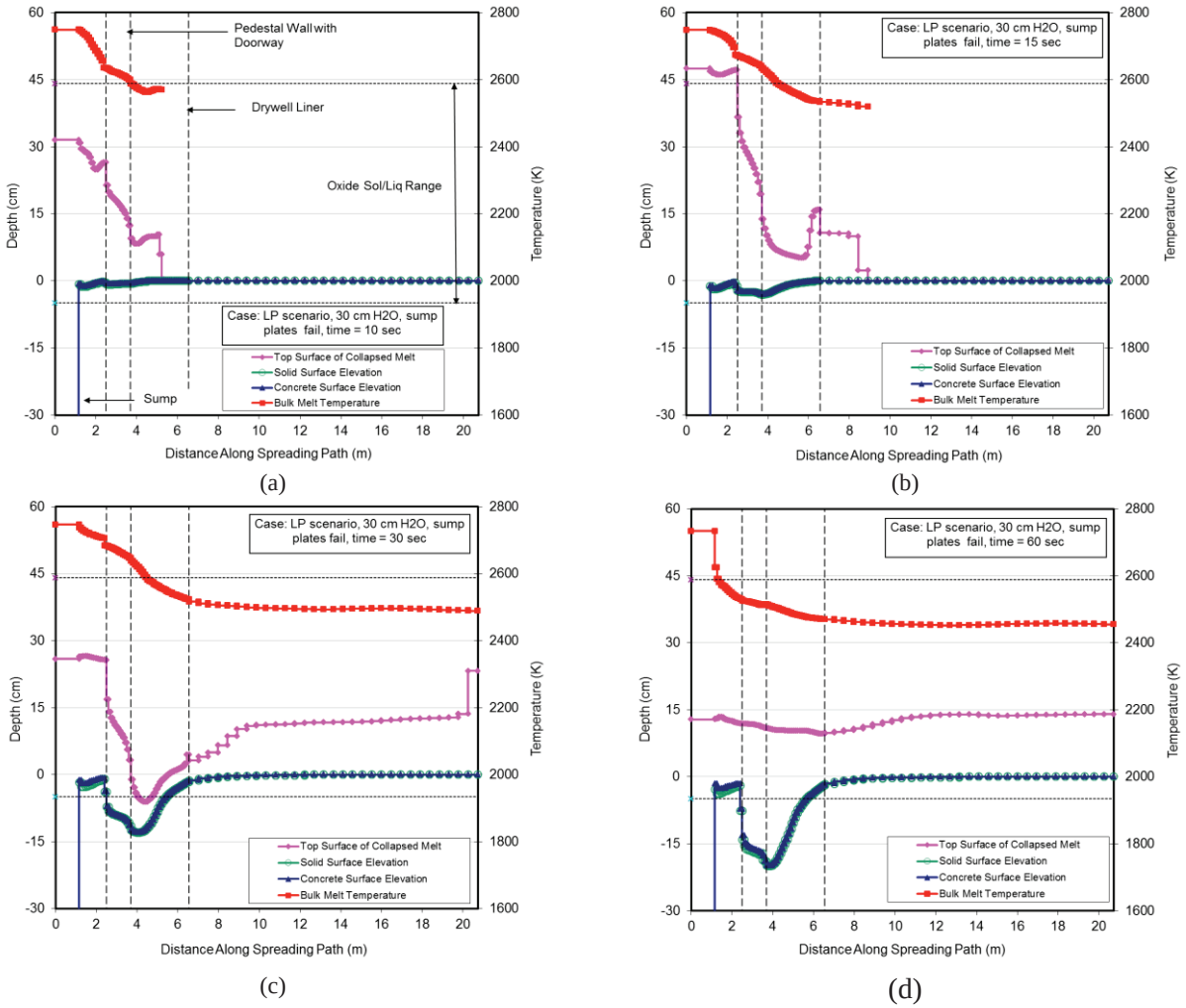

Figure 4. (a-d) Temperature-Depth Profiles at 10, 15, 30, and 60 sec for MAAP-LP-4 Case.

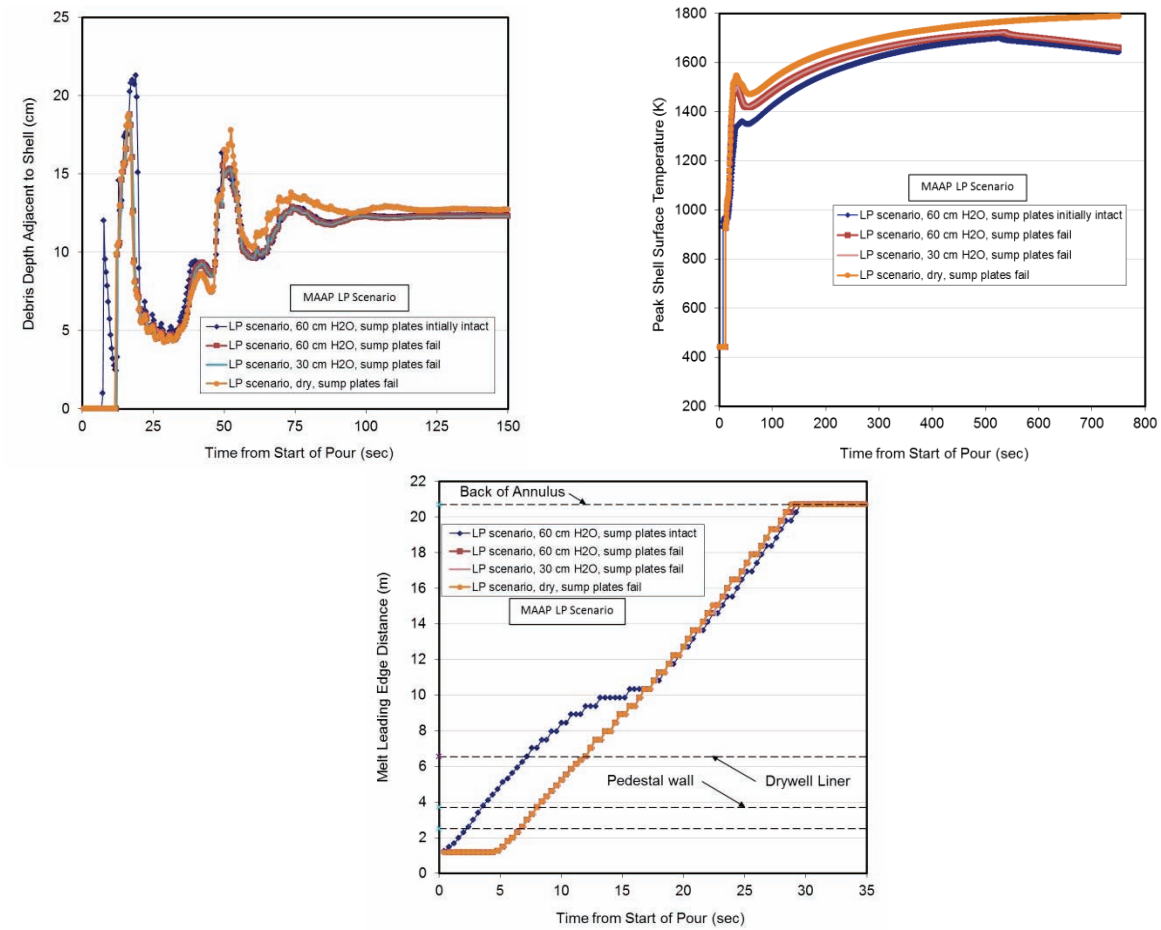

Figure 5. Clockwise from Upper Left: Melt Depth Adjacent to Shell, Peak Shell Temperature, and Melt Leading Edge Location for the four MAAP-LP Cases.

4.3 MAAP High Pressure Scenario

This case involves vessel failure at elevated pressure leading to very rapid discharge of a predominately oxidic core melt into the drywell over a period of ~ 5 seconds (Table I). Consistent with the low-pressure case, the melt is highly superheated with low viscosity, and so the flow is dominated by inertial effects. The MAAP analysis for this case [2] indicates that the cavity is effectively dry at the time of vessel failure. Thus, the best estimate calculation is selected to be the MAAP-HP-3 case (Table IV) in which the sump plates fail at melt contact, and the material spreads into a dry cavity.

As for the low-pressure sequence, due to the high pour rate, the melt rapidly fills the sump volume and then begins to spread out the pedestal doorway, making contact with the shell in ~6 seconds. The melt then begins spreading throughout the annulus, eventually covering the entire floor area in ~ 21 seconds. By two minutes, sloshing has effectively ceased and the debris equilibrates at a uniform level in the pedestal/drywell at ~13 cm. A concrete erosion pocket also forms for this case inside the pedestal doorway and just outside the opening; the peak erosion depth reaches ~ 20 cm by 120 seconds. As previously noted, this localized ablation is caused by high convective heat transfer in this region.

For this high pressure sequence, the shell surface temperature rapidly rises to the steel melting point, eventually leading to melt-through at 286 seconds [13]. The contrast between this prediction and that for

the low-pressure scenario is principally due to the higher melt temperature (~ 50 K) coupled with the higher pour rate that results in greater thermal loading of the shell.

The results for the other three MAAP-HP cases indicate that the overall spreading behavior is not sensitive to the presence/absence of water. As for the low-pressure scenario, this is due to the fact that the energy transport from the vessel during relocation overshadows practically achievable heat removal rates to overlying water, and so the melt is readily able to spread to a uniform melt depth. For the case in which the sump cover plates are initially intact, the debris is able to propagate earlier into the drywell and annulus, but the plates are calculated to be ablated through by 3.58 seconds. However, by this time sufficient corium has accumulated in the pedestal to completely fill the sump, and so the fluid mechanics of the spreading process are not significantly perturbed after the material on top the plates is relocated (dropped by the code) down into the sump.

Aside from spreading behavior, the results show that lack of water in the drywell does not have a significant influence on the shell heat up and ablation rates for this scenario. In particular, failure times for all cases were in the range of 280-290 seconds. Similar to the spreading behavior, this is due to the high impingement heat transfer on the shell in this sequence that overshadows heat removal rates by fin cooling to overlying water.

5. CONCLUSIONS

Major core melting, bottom head failure, and corium-concrete interaction have been predicted at Fukushima Daiichi Unit 1 (1F1) by several different system-level code analyses. Although these codes, such as MELCOR v2.1 and MAAP5, are capable of capturing a wide range of accident phenomena, they do not contain detailed models for ex-vessel core melt behavior. However, specialized codes containing more detailed modeling are available for analyzing melt spreading (e.g., MELTSPREAD) as well as long-term molten corium-concrete interaction and debris coolability (e.g., CORQUENCH). On this basis, DOE-NE funded an analysis to further evaluate the ex-vessel core debris location and extent of interaction for Unit 1 using these higher fidelity tools. The high-level objective was to utilize MELTSPREAD and CORQUENCH to provide rigorous "best estimate" predictions and analysis of ex-vessel core melt accident progression and final debris configuration.

Based on 'best-estimate' MELCOR v2.1 and MAAP5 predictions of melt pours for 1F1, MELTSPREAD was used to perform the melt spreading calculations in containment. These analyses were the primary focus of this paper. The results from the MELCOR and MAAP simulations and the subsequent MELTSPREAD simulations were then used as initial and boundary conditions for the long-term debris coolability analysis with CORQUENCH. The results of the CORQUENCH analyses are reported in a companion study [14].

The results of the spreading analysis predict quite different behavior depending upon the pour scenario. For the low-temperature gradual pour predicted by MELCOR, the code predicts lethargic spreading of a highly viscous melt over a period of ~ 4000 seconds. Concrete ablation is minimal in these cases since the high viscosity limits convection from the melt to underlying concrete. Despite the low flow rate, in all cases the melt is predicted to eventually spread through the pedestal doorway and contact the liner. MELTSPREAD predicts that the liner does not fail in this location for the MELCOR simulations. When water is present, core spreading is limited to ~ 33 m^2.

For the high temperature, rapid melt pours predicted by MAAP, MELTSPREAD predicts the sump plates rapidly ablate through in less than 5 seconds. Furthermore, the concrete erosion during spreading was significant with ~ 2 m^3 in the first 2 minutes with a maximum ablation depth of about 20 cm outside the pedestal door. The melt was also predicted to fully cover the pedestal and drywell annulus floor areas

which sum to ~ 111 m^2. Both low and high-pressure MAAP pour sequences were analyzed. The drywell liner was predicted to remain intact for all low-pressure wet cases, and to fail by erosion due to impingement heat transfer from the melt for the high pressure cases.

ACKNOWLEDGMENTS

This work was supported by the US Department of Energy Office of Nuclear Energy (DOE-NE). This support is greatly appreciated.

REFERENCES

1. R.O. Gauntt et al., "Fukushima Daiichi Accident Study," SAND2012-6173, July 2012.
2. D. Luxat and J. Gabor, "Fukushima Technical Evaluation: Phase 1 – MAAP5 Analysis," EPRI Report No. 1025750 (2013).
3. Nuclear Emergency Response Headquarters, Government of Japan, "Report of Japanese Government to the IAEA Ministerial Conference on Nuclear Safety - The Accident at TEPCO's Fukushima Nuclear Power Stations," June 2011.
4. Y. Yamanaka, Tokyo Electric Power Company, Inc., "Research Plan Regarding Improvement of Simulation Code for Understanding the Status of Fuel Debris in the Reactor," International Symposium on the Decommissioning of TEPCO's Fukushima Daiichi Nuclear Power Plant Unit 1-4, Tokyo, Japan, March 14, 2012.
5. H. Bonneville and A. Luciani, "Simulation of the Core Degradation Phase of the Fukushima Accidents using the ASTEC Code," *Nucl. Eng. Des.*, **271**, p. 261 (2014).
6. Tokyo Electric Power Company Inc. (TEPCO), "Amendments to the Estimate Value of the Core Damage Ratio of Unit 1 to 3 of Fukushima Daiichi Nuclear Power Station based on the Measurement of the Containment Atmospheric Monitoring System," press release, Apr. 27, 2011.
7. Tokyo Electric Power Company Inc. (TEPCO), "The Evaluation Status of Reactor Core Damage at Fukushima Daiichi Nuclear Power Station Units 1 to 3," press release handout, Nov. 30, 2011.
8. Tokyo Electric Power Company Inc. (TEPCO), "Various Approaches for Understanding State of Nuclear Fuel," press release handout, Nov. 30, 2011.
9. M. T. Farmer, J. J. Sienicki, and B. W. Spencer, "The MELTSPREAD-1 Computer Code for the Analysis of Transient Spreading in Containments," *Proceedings of ANS Winter Meeting*, Washington D.C., Nov. 11–15, 1990.
10. M. T. Farmer et al., "The MELTSPREAD-1 Code for Analysis of Transient Spreading and Cooling of High-Temperature Melts, Code Manual," EPRI TR-103413 (1993).
11. M. T. Farmer, "The CORQUENCH Code for Modeling of Ex-Vessel Corium Coolability Under Top Flooding Conditions, Code Manual – Version 3.03", OECD/MCCI-2010-TR03, March 2010.
12. M. T. Farmer, "Modeling of Ex-Vessel Corium Coolability with the CORQUENCH Code," *Proceedings ICONE-9*, Nice, France (2001).
13. K. R. Robb, M. W. Francis, and M. T. Farmer, "Enhanced Ex-Vessel Analysis for Fukushima Daiichi Unit 1: Melt Spreading and Core-Concrete Interaction Analyses with MELTSPREAD and CORQUENCH," ORNL/TM-2012/455 (2013).
14. K. R. Robb, M. T. Farmer, and M. W. Francis, "Fukushima Daiichi Unit 1 Ex-Vessel Prediction: Core–Concrete Interaction," NURETH-16, Chicago, IL, August 30-September 4, 2015.
15. T.G. Theofanous et al., "The Probability of Mark-I Containment Failure by Melt-Attack of the Liner", NUREG/Cr-6025, November (1993).
16. M. T. Farmer and S. Basu, "Melt Spreading Code Assessment, Modifications, and Initial Applications to the EPR Core Catcher Design," *Proceedings ICAPP '09*, Tokyo, Japan (2009).

17. C. Journeau, J.-F. Haquet, B. Spindler, C. Spengler, and J. Foit, "The VULCANO VE-U7 Corium Spreading Benchmark," *Progress in Nuclear Energy*, **48**, p**.** 215 (2006).
18. M. Ramacciotti, C. Journeau, F. Sudreau, and G. Cognet, "Viscosity Models for Corium Melts," *Nuclear Engineering and Design,* **204**, p. 377 (2001).
19. R. Bunt et al., "Reactor Safety Gap Evaluation of Accident Tolerant Components and Severe Accident Analysis,"NURETH-16, Chicago, IL, August 30-September 4, 2015.
20. D. Luxat, J. Hanophy, and D. Kalanich, "Electric Power Research Institute, "Modular Accident Analysis Program (MAAP) – MELCOR Crosswalk, Phase 1 Study," EPRI Report No. 3002004449 (2014)
21. C. C. Chu, J. J. Sienicki, and B.W. Spencer, "The Effects of Below-Vessel Structure and Water on Ex-Vessel Melt Arrival Conditions in a MARK I Containment," *Proceedings NURETH-5*, Salt Lake City, UT, September 21-24 (1992).